Small Signal Modeling of Series Resonant Converter based on State-plane Analysis

Vishal Anand A G*, Utsab Kundu†, Ranganathan Gurunathan*, Kaushik Basu†
*Bloom Energy (I) Pvt Ltd, Bangalore
{vanand,rgurunat}@bloomenergy.com
†Department of Electrical Engineering, Indian Institute of Science, Bangalore
{utsabkundu,kbasu}@iisc.ac.in

IECON 2021 - 47th Annual Conference of the IEEE Industrial Electronics Society | 978-1-6654-3554-3/21/$31.00 ©2021 IEEE | DOI: 10.1109/IECON48115.2021.9589595

***Abstract*—In this paper, small signal modeling of series resonant converter (SRC) operating under variable frequency modulation is presented. Noting that the existing small signal models are of higher order and mathematically complex, a reduced order model is proposed to make the control loop design easy. Both time-domain-based exact state plane analysis and averaging technique of an electrical variable are adopted to derive control-to-output transfer functions of SRC. Accuracy of the proposed approach is validated using LTSPICE simulation.**

***Index Terms*—Averaging Technique, Series Resonant Converter, Small Signal Modeling, state-plane Analysis, Variable Frequency Modulation**

I. Introduction

Isolated DC-DC converters today find their use in a variety of applications like Electric traction [1], grid integration of renewable energy sources [2] and other power supplies. For these applications, resonant mode power conversion topologies viz. series resonant converter (SRC) [3] and parallel resonant converter (PRC) [4] have gained lot of attention due to their inherent features like soft-switching, low electromagnetic interference (EMI) emission etc. Closed loop control of resonant converters is typically implemented either using variable frequency modulation (VFM) or constant frequency phase shift modulation (PSM) [5]. For many applications of SRC, VFM-based closed loop control is preferred since this technique offers lower rms current in the resonant tank compared to its PSM-based counterpart [6]. However, a clear insight on small signal behavior of frequency modulated SRC is necessary for the controller design.

A number of techniques are available in literature to perform small signal modeling of SRC [7]–[10]. An approximate approach [7] models SRC as a 3-pole system, where the low-frequency pole is due to the filter and load network. To model the resonant behavior, this method introduces a double-pole at the beat frequency ($f_s - f_b$), where f_s denotes steady-state switching frequency and f_b represents the resonant frequency. But this model is derived intuitively based on earlier reported experimental results and also some of the model parameters are determined empirically. The modeling technique based on extended describing functions (EDF) [8] first decomposes the state variables of SRC into sine and cosine terms. Next, by applying harmonic balance on the nonlinear state equations, this method derives a fifth-order model which complicates the closed loop controller design. Since this technique is based on fundamental harmonic approximation (FHA), the accuracy of this approach is questionable at light load conditions due to significant higher order resonant current harmonics. A third-order small signal model is proposed in [9], which though arrives at the same transfer function as in [7], but mitigates the requirement of estimating parameters using simulation/experimental results. But this technique being an extension of the EDF-based method, the effects of higher order harmonics are not considered here as well. A communication signal theory based approach [10] successfully derives a small signal equivalent circuit model of SRC, which is certainly useful for SPICE simulation. But no closed form solution for control-to-output transfer function is provided. Using the fundamentals of steady-state state-plane analysis of SRC [11], a discrete time-domain-based small signal model is presented in [12]. Similar to most of the existing approaches, this method also suffers from mathematical complexity and fails to derive a simplified small signal model. However, averaging of state variables is a widely used technique for pulse-width modulated (PWM) converters, but this approach is typically not applied to any resonant converter [13].

This paper presents a new small signal modeling approach for SRC, which is based on both state-plane analysis and averaging of a electrical variable over the switching period. The key contributions of this paper are as follows. (a) Averaging technique is adopted to model the filter and load network of SRC. (b) Reduced order control-to-output transfer functions are derived, which are extremely useful for control loop design. (c) The coefficients of these transfer functions are obtained using exact solutions of steady-state equations, using state-plane analysis. The remaining part of the paper is organized as follows. Section II analyzes the steady-state behavior of SRC using state-plane method. Small signal model of SRC is derived in section III. Simulation results are showcased in Section IV and Section V concludes the paper.

II. Steady State Analysis

Fig. 1 depicts the power train of an SRC, where L_r, C_r and n represent the resonant inductance, capacitance and the transformer turns ratio, respectively. Conventional variable switching frequency based closed loop control architecture is also shown in Fig. 1. In this configuration, the controller acts

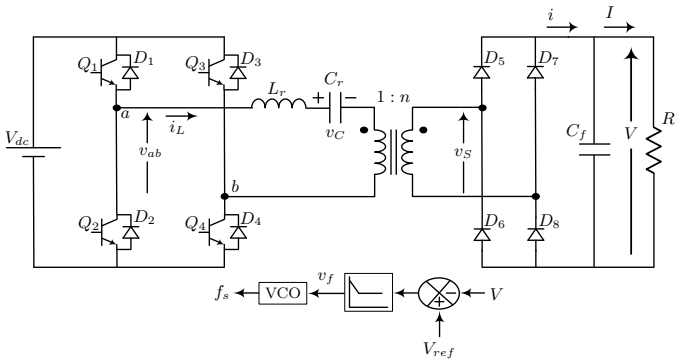

Fig. 1. SRC with variable switching frequency control.

on the difference between reference voltage (V_{ref}) and output voltage feedback (V). The output of the controller, v_f, is fed to a voltage controlled oscillator (VCO) which decides the switching frequency (f_s) of the primary side H-bridge. The primary H-bridge is switched to apply a square wave voltage across terminals a-b of amplitude V_{dc} and frequency f_s. This VFM-based control structure ensures that the output voltage is held constant under input voltage and/or load variations. The exact time domain analysis of SRC operating under VFM is performed using a two-step approach [14]. Firstly, neglecting all the circuit non-idealities, the complete switching cycle is divided into multiple operating modes based on piece-wise linear sub-circuits. Then state-plane method is adopted to determine the mode boundaries. To find an important relation used in deriving the parameters of the small signal model developed in next section, the analysis is presented briefly as follows.

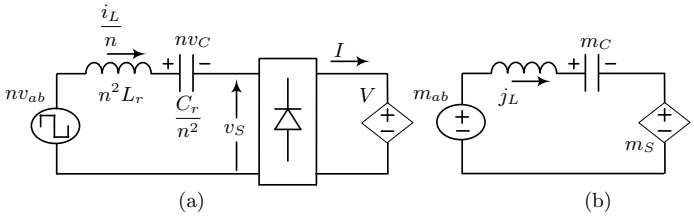

Fig. 2. Series Resonant DC-DC converter. (a) Equivalent circuit reflected at transformer secondary. (b) Per-unitized equivalent circuit.

Fig. 2(a) shows the equivalent circuit of SRC reflected at transformer secondary. For simplicity of the analysis, the relevant parameters are converted in per unit (PU) form. The base quantities are provided in Table I and the PU quantities are listed in Table II. Using these parameters, a normalized equivalent circuit is derived and shown in Fig. 2(b) where the load along with the output filter capacitor and diode bridge is represented as a current dependent voltage source. Here, m_{ab} and m_S represent normalized tank input and transformer secondary voltage, respectively while j_L and m_C are PU inductor current and capacitor voltage. The complete switching cycle of SRC under steady-state operation is divided into 4 distinct modes based on the sign of m_{ab} and j_L. While deducing these modes, continuous conduction mode (CCM) operation and above resonance ($F > 1$) condition are considered, where F is the PU switching frequency and $\gamma = \pi/F$ as given in Table II. Fig. 3 shows normalized equivalent circuits during each of these modes. Normalized state equations during these modes are given in Table III. The electrical variables of SRC during steady-state operation are depicted in Fig. 4 as a function of

TABLE I
PER-UNITISATION BASE PARAMETERS

Description	Formula
Base Voltage, V_b	nV_{dc}
Base Impedance, R_b	$n^2\sqrt{L_r/C_r}$
Base Current, I_b	V_b/R_b
Base Frequency, f_b	$1/2\pi\sqrt{L_rC_r}$

TABLE II
PU QUANTITIES

Description	Formula
Resonant capacitor voltage, m_C	nv_C/V_b
Resonant inductor current, j_L	i_L/nI_b
Switching frequency, F	f_s/f_b
Rectifier input voltage, m_S	v_S/V_b
Angular half-period, γ	π/F
Rectified current, j	i/I_b
Output current, J	I/I_b
Output Voltage (or Voltage gain), M	V/V_b
Angular frequency, ω_b	$2\pi f_b$
Angle variable, θ	$\omega_b t$
Tank Voltage, m_{ab}	nv_{ab}/V_b
Load Resistance, Q	R_b/R
Output Filter Capacitance, K	$1/(\omega_b R_b C_f)$

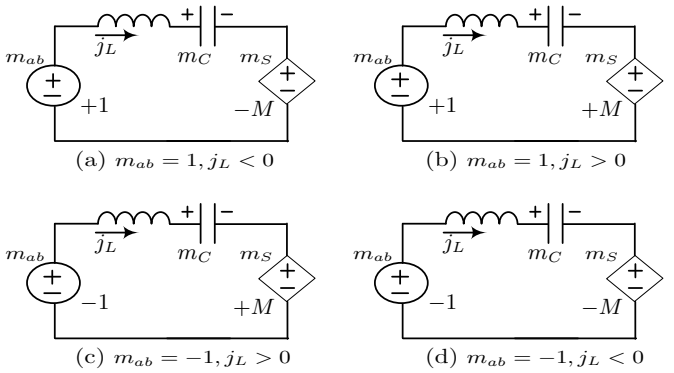

Fig. 3. Normalized equivalent circuit of SRC under different operating modes. (a) Mode 1, (b) Mode 2, (c) Mode 3 and (d) Mode 4.

TABLE III
STATE EQUATIONS

Mode	Governing State Equation
1	$\frac{dj_L}{d\theta} + m_C = 1 + M$
2	$\frac{dj_L}{d\theta} + m_C = 1 - M$
3	$\frac{dj_L}{d\theta} + m_C = -1 - M$
4	$\frac{dj_L}{d\theta} + m_C = -1 + M$

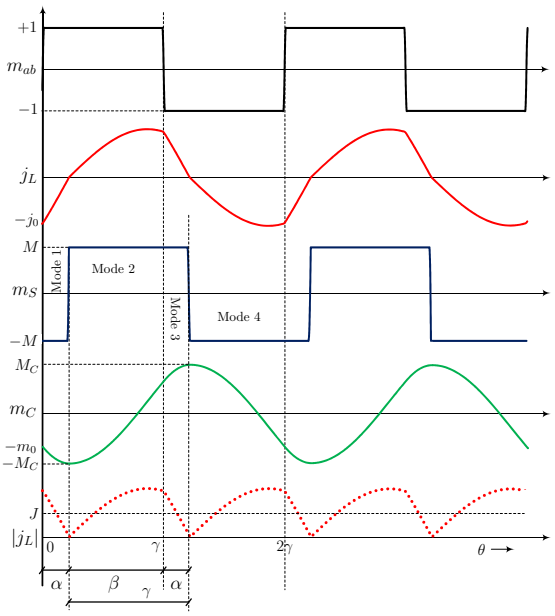

Fig. 4. Key waveforms of SRC as a function of angle variable, θ.

the angle variable, θ and different modes are also highlighted. Modes 1,3 and 2,4 are symmetrical and their periods are α and β respectively, so half period is defined by $\gamma = \alpha + \beta$. Normalized rectified resonant inductor current is denoted as $|j_L|$ in Fig. 4. The average of this current, J, flows into the load due to charge balance of filter capacitor, C_f, over a switching period. Since j_L flows through the resonant capacitor as well, normalized load current (J) is derived as

$$J = \frac{1}{\gamma}\int_{\alpha}^{\alpha+\gamma} j_L d\theta = \int_{\alpha}^{\alpha+\gamma} \frac{dm_C}{d\theta} d\theta, \tag{1}$$

where, α and $\alpha + \gamma$, refer to the instants where Modes 1 and 3 terminate, respectively, as indicated in Fig. 4. During Modes 2 and 3, capacitor voltage changes from negative to positive peak and due to symmetry both peaks have same magnitude M_C. Rearranging (1), a relationship between PU peak capacitor voltage, M_C, and J is expressed as

$$M_C = \frac{J\gamma}{2}. \tag{2}$$

The variations in j_L and m_C are plotted in Fig. 5 against each other as the angle variable, θ evolves. The circular arc corresponding to Mode 1 begins at the point in the 3rd quadrant $[-m_0, -j_0]$. From the solution of the equivalent circuit shown in Fig. 3(a), the variation in $j_L(\theta)$ with respect to m_C is plotted. The center of this circle is $[-1-M, 0]$ and the radius of the circular arc is r_1. Mode 1 ends when $j_L = 0$ and $m_C = -M_C$. Mode 2 begins here and the center of the circle changes to $[-1+M, 0]$ and the radius changes to r_2. This mode ends when the angle variable, $\theta = \gamma$. Modes 3 and 4 are symmetric to Modes 1 and 2 as explained earlier. Since Mode 1 ends at $j_L = 0, m_C = -M_C$, we can write the following expressions from Fig. 5.

$$r_1 = M_C - 1 - M, \quad r_2 = M_C - 1 + M. \tag{3}$$

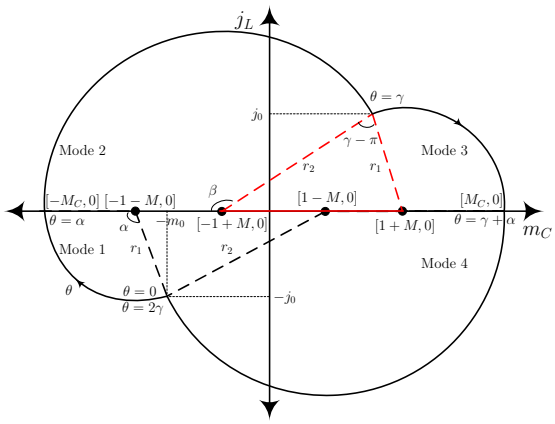

Fig. 5. state-plane portrait of the Series Resonant Converter.

Applying Law of Cosines on the triangle highlighted in dotted red line in Fig. 5, the following expression is obtained.

$$(2)^2 = r_1^2 + r_2^2 - 2r_1 r_2 \cos(\gamma - \pi). \tag{4}$$

Using (2)-(4) and since $\gamma = \pi/F$, a relationship between M, F and J is derived.

$$J^2 + J\left(\frac{4F}{\pi}\right) + \frac{4F^2(M^2-1)}{\pi^2}\tan^2\left(\frac{\pi}{2F}\right) = 0. \tag{5}$$

Considering steady-state CCM operation of SRC, a similar expression can be derived for $F < 1$ condition as well. Considering only the positive real root of (5), J is expressed as a function of M and F as

$$J = g(M, F) = \frac{2pF}{\pi}\left[\frac{\sqrt{1 - M^2\sin^2\frac{\pi}{2F}}}{\cos\frac{\pi}{2F}} - 1\right]. \tag{6}$$

It is interesting to note that eq. (6) is valid for both above ($F > 1$) and below ($F < 1$) resonance conditions and accordingly the quantity, p, is defined as

$$\begin{cases} p = -1, \; F < 1 \\ p = +1, \; F > 1 \end{cases}$$

III. Small Signal Analysis

Similar to PWM converters, a simple small signal model linearized around a quiescent operating point is desired for SRC as well. To achieve this goal, the first step is to reiterate that the PU rectifier output current averaged over a switching cycle is equal to the normalized load current (J) during steady-state operation. Therefore, the quantity, J, in (6) certainly represents the average rectifier output current in normalized form. Based on this consideration, the output filter and load of the SRC is shown in Fig. 6, where, C_f, is the filter capacitor, R is the load and i is the rectifier output current as shown in Fig. 1.

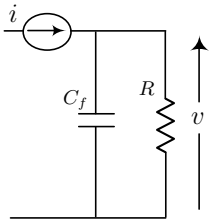

Fig. 6. Output Filter and load of SRC.

A. Average model of filter and load

Denoting average output voltage as $\overline{v}$ and average rectifier output current as $\overline{i}$, Kirchhoff's Current Law (KCL) is applied at the input node of the filter network shown in Fig. 1.

$$C_f \frac{d\overline{v}}{dt} = \overline{i} - \frac{\overline{v}}{R}. \tag{7}$$

Per-unitizing (7) using Table I we can arrive at the following expression where, Q is the PU load resistance and K is defined in Table II.

$$K\frac{dM}{dt} = J - QM. \tag{8}$$

The same relationship holds good for any small signal perturbation in J, ΔJ, and produces small signal variation in M, ΔM accordingly. Applying Laplace transforms on both sides and rearranging (8), the small signal output transfer function of the SRC is expressed as

$$\frac{\Delta M(s)}{\Delta J(s)} = \frac{1}{sK+Q}. \tag{9}$$

B. Small signal perturbation in $g(M, F)$

By perturbing (6) while considering only linear terms [15] and taking Laplace transforms one gets (10) where A and B are defined in (11) and (12) respectively. C is defined in (13) for the brevity of expressions A and B.

$$\Delta J(s) = B\Delta M(s) + A\Delta F(s), \tag{10}$$

$$A = \frac{\partial g}{\partial F} = \frac{2p}{\pi}\left(\frac{C}{\cos\frac{\pi}{2F}} - 1\right) + \frac{p}{2F}\left[\frac{(M^2-1)\sin\frac{\pi}{F}}{C\cos^3\frac{\pi}{2F}}\right]. \tag{11}$$

$$B = \frac{\partial g}{\partial M} = -\frac{2pFM}{\pi}\left[\frac{\sin^2\frac{\pi}{2F}}{C\cos\frac{\pi}{2F}}\right]. \tag{12}$$

$$C = \sqrt{1 - M^2\sin^2\frac{\pi}{2F}}. \tag{13}$$

Considering (9) and (10), a small signal block diagram representation of SRC is derived and presented in Fig. 7. Substituting $\Delta M(s)$ from (9) into (10), small signal normalized transfer function of rectifier output current to switching frequency is expressed as

$$\frac{\Delta J(s)}{\Delta F(s)} = \frac{(sK+Q)A}{sK+(Q-B)}. \tag{14}$$

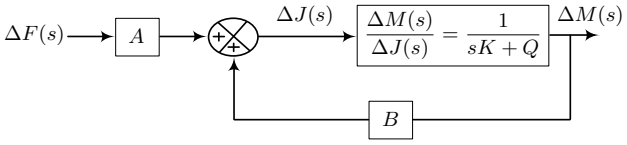

Fig. 7. Small signal block diagram of SRC.

Similarly, substituting $\Delta J(s)$ from (9) into (10), small signal normalized transfer function of output voltage to switching frequency is obtained as

$$\frac{\Delta M(s)}{\Delta F(s)} = \frac{A}{sK+(Q-B)}. \tag{15}$$

It is worth mentioning here that the first-order small signal models, (14) and (15), are extremely useful for current and voltage control loop design, respectively. Eq. (14) and (15) along with the A and B coefficients present a complete small signal model of CCM operated SRC for both above ($F > 1$) and below ($F < 1$) resonance conditions. In order to use these transfer functions for closed loop control design, it's important to convert the PU based transfer function to actual small signal transfer functions as given below.

$$\frac{\Delta i(s)}{\Delta f_s(s)} = \frac{(sK+Q)AI_b}{sK+(Q-B)}. \tag{16}$$

$$\frac{\Delta v(s)}{\Delta f_s(s)} = \frac{AV_b}{sK+(Q-B)}. \tag{17}$$

where, Δi, Δv and Δf_s are the small signal perturbations of the rectified current, i, output voltage, v and switching frequency, f_s respectively. It is appropriate to highlight here that no additional assumption has been made during the proposed small signal analysis. However, this approach inherently assumes that the steady-state time-domain relationship, given by (6), is valid under small signal perturbation in the switching frequency. The dynamics of averaged resonant capacitor voltage and inductor current is neglected. Even during small signal perturbation, half wave symmetry of these waveforms are approximately maintained and the average remains close to zero.

IV. Simulation results

The power circuit of an SRC is developed using LTSPICE simulation software. Input/output specifications of the converter and different circuit parameters are detailed in Table IV. Considering these parameters and using the definitions, listed in Table I, different base quantities are calculated and presented in Table IV. For the given transformer turns ratio and fixed input/output specifications, the normalized output voltage (M) remains constant at 0.675. So, for any given F, the quantity, J, gets automatically defined by (6). The required load resistance (R) for simulation is determined using the following steps. Firstly, for a given steady-state normalized switching frequency (F), J is calculated using (6) and $M = 0.675$. Next, applying charge balance on filter capacitor (C_f), normalized load resistance (Q) is expressed as

$$Q = \frac{J}{M}. \tag{18}$$

TABLE IV
SRC SPECIFICATIONS AND PARAMETERS

Description	Value
Input Voltage, V_{dc}	400 V
Output Voltage, V	375 V
Output Power, P	8.2 kW
Resonant Inductance, L_r	65.4 μH
Resonant Capacitor, C_r	172 nF
Filter Capacitor, C_f	1 mF
Transformer turns, $1:n$	25:18
Base Resistance, R_b	37.6 Ω
Base Current, I_b	14.7 A
Base Frequency, f_b	47.5 kHz

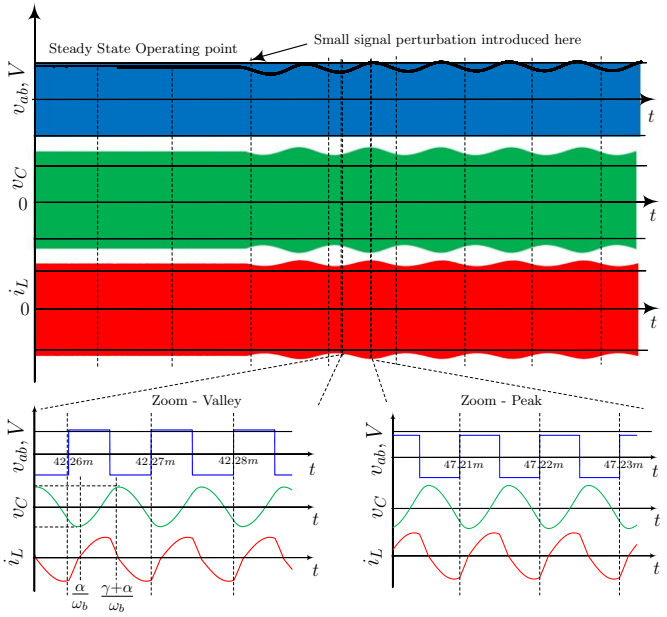

Fig. 8. Variation in different electrical variables due to small signal perturbation in switching frequency. Scale: V, v_{ab} (400V/div), i_L (30A/div), v_C (400V/div). X-axis: Normal (10ms/div), Zoomed (10μs/div).

Subsequently, using (18) and the base resistance, listed in Table IV, required load (R) for simulation is obtained.

Open loop AC simulation is performed in LTSPICE by sweeping the switching frequency using a VCO. The VCO control input, V_f, defines the normalized switching frequency (F) at steady-state. The VCO is considered to be linear, which means that any VCO input, $v_f = V_f + \Delta V_f \sin\omega_m t$, results in frequency output, $f = F + \Delta F \sin\omega_m t$. Here, ω_m represents the angular sweep frequency and ΔV_f and ΔF define small signal perturbations at the VCO input and PU switching frequency, respectively. Subsequently, the transfer characteristics with respect to the VCO input is considered as the benchmark for validating the proposed modeling approach. As discussed in Section III-C, half-wave symmetry of the resonant capacitor voltage, v_C, under small signal perturbation is an inherent assumption of the proposed approach. To validate this, a small

TABLE V
HALF-WAVE SYMMETRY DURING SMALL-SIGNAL PERTURBATION

Description	Zoom-Valley	Zoom-Peak
Negative Peak Voltage, $-M_C V_b$	$-450V$	$-530V$
Positive Peak Voltage, $M_C V_b$	$450V$	$530V$

signal perturbation of 100 Hz is added with the nominal VCO input and the corresponding waveforms of different electrical variables of SRC are presented in Fig. 8. Small signal variation in the output voltage, V, and small signal envelope in the state variables (i_L and v_C) are clearly visible. Zoomed views of these switching waveforms both at the peak and the valley of the envelope are also shown in Fig. 8. Magnitudes of capacitor voltage at $t = \alpha/\omega_b$ and $t = (\gamma+\alpha)/\omega_b$ are measured and presented in Table V. Evidently, half-wave symmetry in v_C is maintained both at the peak and the valley of the small signal perturbation.

Using the frequency sweep scheme developed in LTSPICE, small signal transfer characteristics of SRC are obtained for the following steady-state operating points above resonance, $F = 1.2$, 1.3. In order to maintain the same output voltage, M, the Q value is adjusted at each operating frequency, F. Using (17), output voltage to switching frequency ($\Delta v(s)/\Delta f_s(s)$) characteristics are determined and presented along with the corresponding simulation results in Fig. 9(a). Excellent agreement between analytical and simulation results are noted approximately till the modulation frequency is (1/10)th of the steady-state switching frequency (f_s). Similarly, transfer characteristics of rectifier output current to switching frequency ($\Delta i(s)/\Delta f_s(s)$) are obtained using (16) and plotted together with the simulation results in Fig 9(b). Close agreement between analytical data and simulation results is evident here as well. To validate the proposed model below resonance, a couple of steady-state operating points, $F = 0.7$, 0.8, are chosen. Similar to above resonance, the Q value is adjusted to maintain the same M. Considering these points, analytical and simulated characteristics of $\Delta v(s)/\Delta f_s(s)$ and $\Delta i(s)/\Delta f_s(s)$ are presented in Fig 9(c) and Fig 10, respectively. These results confirm that the proposed approach is valid till the modulation frequency is nearly equal to f_s/10 during below resonance conditions as well. A summary of the location of the poles and zeroes for the derived transfer functions and its variation as a function of switching frequency is provided in Table VI.

V. CONCLUSION

To address the existing problem of mathematically complex and higher order small signal models, a reduced order model-

TABLE VI
TRANSFER FUNCTION VARIATION WITH SWITCHING FREQUENCY

Description	$F = 1.2$	$F = 1.3$	$F = 0.8$	$F = 0.7$
Pole Location, Hz	19.6	13.7	13.9	8.1
Zero Location, Hz	9.3	6.2	9.7	6.6
$\Delta v(s)/\Delta f_s(s)$ Gain, dB	59.0	55.0	62.0	59.8
$\Delta i(s)/\Delta f_s(s)$ Gain, dB	34.2	26.7	37.7	32.1

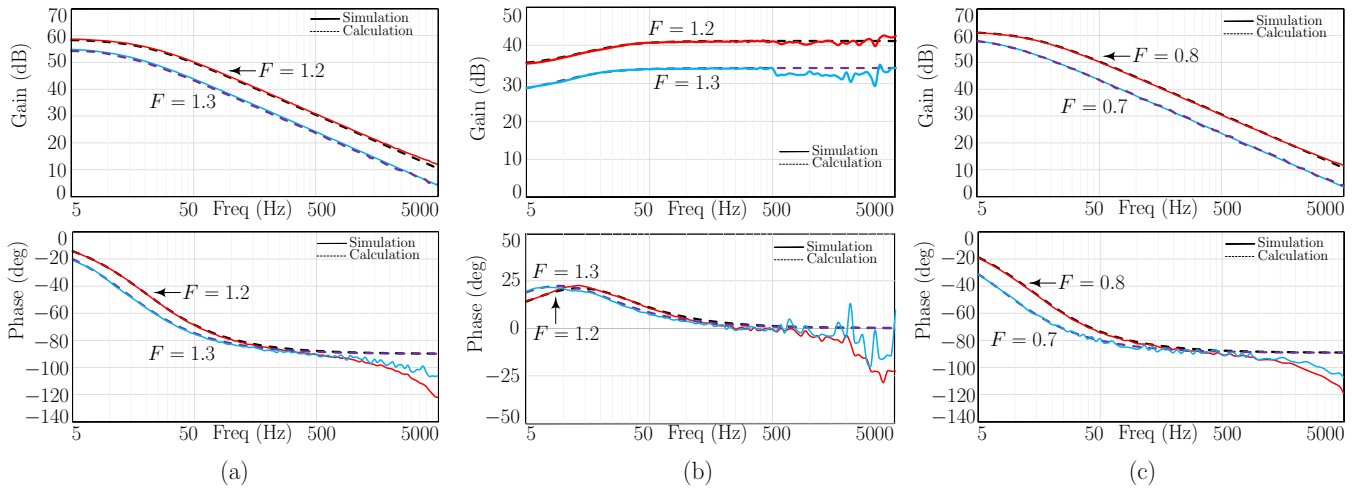

Fig. 9. Small signal transfer functions of the SRC (a) Gain-phase plot of $\Delta v(s)/\Delta f_s(s)$ - Above resonance (b) Gain-phase plot of $\Delta i(s)/\Delta f_s(s)$ - Above resonance and (c) Gain-phase plot of $\Delta v(s)/\Delta f_s(s)$ - Below resonance

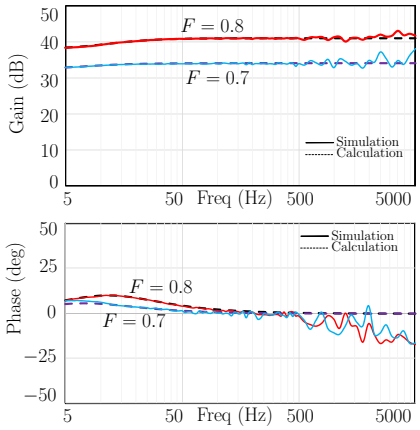

Fig. 10. Gain-phase plot of $\Delta i(s)/\Delta f_s(s)$ - Below resonance

ing approach for SRC is presented in this paper. The proposed technique exploits the steady-state state-plane analysis of SRC and introduces averaging technique of an electrical variable to arrive at a first-order small signal model. Closed form transfer functions of rectifier output current to switching frequency and output voltage to switching frequency are derived. This method not only makes voltage mode controller design easy but opens up an opportunity for rectifier output current feedback based nested loop design as well. Simulation results from LTSPICE validate the approximation made with regards to the half-wave symmetry in the resonant tank inductor current and capacitor voltage. Analytical data are noted to be in well agreement with the simulation results till the modulation frequency is (1/10)th of the steady-state switching frequency. This clearly defines the scope of the proposed model. However, extension of this modeling strategy to facilitate high bandwidth controller design can certainly be explored in future.

REFERENCES

[1] M. T. Outeiro, G. Buja, and D. Czarkowski, "Resonant power converters: An overview with multiple elements in the resonant tank network," *IEEE Industrial Electronics Magazine*, vol. 10, no. 2, pp. 21–45, June 2016.

[2] D. V. S. Kouro, J. I. Leon and L. G. Franquelo, "Grid-connected photovoltaic systems: An overview of recent research and emerging pv converter technology," *IEEE Industrial Electronics Magazine*, vol. 9, no. 1, pp. 47–61, March 2015.

[3] C. Yeh, C. Chen, M. Lee, and J. Lai, "A hybrid modulation method for single-stage soft-switching inverter based on series resonant converter," *IEEE Transactions on Power Electronics*, vol. 35, no. 6, pp. 5785–5796, 2020.

[4] D. G. Bandeira, T. B. Lazzarin, and I. Barbi, "High voltage power supply using a t-type parallel resonant dc dc converter," *IEEE Transactions on Industry Applications*, vol. 54, no. 3, pp. 2459–2470, 2018.

[5] Y. Chen, J. Xu, Y. Wang, L. Lin, and J. Cao, "A dual-carrier modulation technique for half-bridge resonant converter with wide soft-switching range," *IEEE Transactions on Industrial Electronics*, vol. 66, no. 1, pp. 223–232, 2019.

[6] C.-S. Yeh, C.-W. Chen, M. Lee, and J.-S. Lai, "A hybrid modulation method for single-stage soft-switching inverter based on series resonant converter," *IEEE Transactions on Power Electronics*, vol. 35, no. 6, pp. 5785–5796, 2020.

[7] V. Vorperian, "Approximate small-signal analysis of the series and the parallel resonant converters," *IEEE Transactions on Power Electronics*, vol. 4, no. 1, pp. 15–24, 1989.

[8] E. Yang, F. Lee, and M. Jovanovic, "Small-signal modeling of series and parallel resonant converters," in *[Proceedings] APEC '92 Seventh Annual Applied Power Electronics Conference and Exposition*, 1992, pp. 785–792.

[9] S. Tian, F. C. Lee, Q. Li, and B. Li, "Small-signal equivalent circuit model of series resonant converter," in *2015 IEEE Energy Conversion Congress and Exposition (ECCE)*, 2015, pp. 172–179.

[10] S. Lineykin and S. Ben-Yaakov, "A unified spice compatible model for large and small signal envelope simulation of linear circuits excited by modulated signals," in *IEEE 34th Annual Conference on Power Electronics Specialist, 2003. PESC '03.*, vol. 3, 2003, pp. 1205–1209 vol.3.

[11] R. Oruganti and F. C. Lee, "Resonant power processors, part i—state plane analysis," *IEEE Transactions on Industry Applications*, vol. IA-21, no. 6, pp. 1453–1460, 1985.

[12] K. Siri, C. Lee, and S. Fang, "Frequency response of resonant converters," in *[Proceedings] IECON '90: 16th Annual Conference of IEEE Industrial Electronics Society*, 1990, pp. 944–949 vol.2.

[13] A. Tahavorgar and J. E. Quaicoe, "Stability and small-signal analyses of the dual series-resonant dc dc converter," *IEEE Transactions on Power Electronics*, vol. 34, no. 2, pp. 1420–1430, 2019.

[14] A. Wittulski and R. Erickson, "Steady-state analysis of the series resonant converter," *IEEE Transactions on Aerospace and Electronic Systems*, vol. AES-21, no. 6, pp. 791–799, 1985.

[15] R. W. Erickson and D. Maksimovic, *Fundamentals of Power Electronics*, 2nd ed. Springer, 2001.